Metal-Decorated Silicene for Hydrogen Storage

Shaira Jehsarine C. Narido[1,*] and Nelson B. Arboleda Jr.[1,2]

[1] *Physics Department, De La Salle University, 2401, Taft Avenue, Manila*
[2] *DLSU-Science and Technology Complex, Biñan, Laguna*
*Corresponding Author: shaira.narido@dlsu.edu.ph

Abstract: Environmental and energy security concerns makes renewable energy research imperative. A key issue that needs to be addressed before the implementation of a renewable energy system is the issue of energy storage, in which materials-based hydrogen storage is considered as an option. In this paper, the metal-decorated silicene was studied for hydrogen storage applications. These were performed using the Vienna Ab Initio Simulation Package (VASP), a plane wave-based code. The potential was described using the projector-augmented wave (PAW) method. The exchange-correlation energy was approximated using Generalized Gradient Approximation (GGA) functional in the Perdew, Burke, and Ernzerhof (PBE) form. The k points were gamma-centered and automatically generated using the Monkhorst-Pack scheme. The energy cutoff, number of k points, vacuum spacing, silicene lattice constant, and silicene buckling height were determined using various convergence tests. The transition metals Co, Ni, Pd, and Pt were used for the metal decoration. Relaxation calculations were done to determine the most stable adsorption site for the metal adatoms. Results show the hollow site to be the most stable among the four adsorption sites (bridge, hollow, top, and valley). Static calculations with Pd and Pt decoration also confirmed this.

Key Words: Hydrogen Storage; Silicene; Metal Decoration, Adsorption

1. INTRODUCTION

The continuous increase in world energy demand and the negative impact of fossil fuel sources in the environment creates a need for diversifying energy sources (Höök & Tang, 2013; IEA, 2014). The most preferable alternative is a renewable energy source which produces little or no emissions such as solar or wind power. However, the power output of these sources may be become unstable because of unfavorable weather conditions such as cloudy weather or low wind speed. Hence, there is a need for an effective energy storage method so that renewable systems can provide a steady supply of energy even during these periods (Converse, 2006). One of the alternatives for effective energy storage is through the use of hydrogen, an energy carrier.

As an energy carrier, hydrogen can be used as energy source by conversion to heat or electricity via combustion or electrochemical reactions (Pudukudy, Yaakob, Mohammad, Narayanan, & Sopian, 2014). Its combustion produces water and no harmful emissions except NO_x compounds (Cipriani et al., 2014; Midilli & Dincer, 2008; Momirlan & Veziroglu, 2005; Najjar, 2013; Pudukudy et al., 2014; Sharaf & Orhan, 2014) which can be remedied by modifying the engine design (Momirlan & Veziroglu,

2005). This makes hydrogen a suitable energy carrier for a greener energy system

Hydrogen has 143 MJ·kg⁻¹ energy weight density—about three times the weight density of liquid hydrocarbon fuels. However, gaseous hydrogen has low energy volumetric density of 0.0107 MJ·L⁻¹. Physical storage through liquid hydrogen (LH₂) is also expensive (Najjar, 2013) and has problems with leakage (Cipriani et al., 2014; Najjar, 2013), which raises issues on the safety of LH₂ storage.

An alternative to physical storage is materials-based hydrogen storage through chemical hydrides and adsorption materials (Cipriani et al., 2014; Durbin & Malardier-Jugroot, 2013; Najjar, 2013; Pudukudy et al., 2014), which is relatively safer (Pudukudy et al., 2014). One of the popular materials actively studied in this field are carbon nanomaterials (Pudukudy et al., 2014), where many hydrogen storage studies has been conducted (Gopalsamy & Subramanian, 2014; Ströbel, Garche, Moseley, Jörissen, & Wolf, 2006; Wang et al., 2013a; Yang, Jung, Kim, & Park, 2012; Züttel, Wenger, Sudan, Mauron, & Orimo, 2004). Examples of nanomaterials include nanotubes, nanoflowers, nanobamboos, graphene, and many others. Calculations for hydrogen storage capacities give of 3 to 14 wt% storage, but experiments currently yield 0 to 3 wt % storage (Ströbel et al., 2006).

Many studies on CNTs and graphene showed that metal adsorption and doping could improve the hydrogen storage capacity of carbon nanomaterials (Ströbel et al., 2006). Metals that were used for improving the hydrogen storage capacity of graphene include alkali metals, alkaline earth metals, and transition metals (Chen et al., 2013; Choi, Min, Gwak, Paek, & Oh, 2014; Chu, Hu, Hu, Yang, & Deng, 2011; Gao et al., 2012; Guo et al., 2013; Kim, Lee, Hwang, Yun, & Chung, 2014; Li et al., 2012; Ma, Zhang, Xu, & Ji, 2014; Nachimuthu, Lai, & Jiang, 2014; Sigal, Rojas, & Leiva, 2011; Yadav, Zhu, & Singh, 2014; Zhou et al., 2014). Hydrogen molecules were found to have Coulombic or Kubas interaction with these metal dopants, whose binding energies allow for relatively high hydrogen storage (Wang et al., 2013a). In another mechanism called "spillover effect", transition metals act as catalyst for hydrogen dissociation. The dissociated hydrogen atoms then forms bonds with carbon atoms and is said to have "spilled over" the carbon nanomaterial (Ströbel et al., 2006; Wang et al., 2013b). However, one problem is that metal adatoms tend to cluster on graphene, which significantly lowers the storage capacity. Calculations showed that this can be remedied by substitutional doping of graphene with nitrogen or boron (Nachimuthu et al., 2014).

Recently, the silicon analog of graphene,

silicene, was fabricated (Vogt et al., 2012). Metal adsorption studies showed stronger binding of metal adatoms with silicene as compared with graphene (Lin & Ni, 2012). Moreover, the metal-silicene binding energies are stronger than the cohesive energies of these metals. This means that silicene will not encounter the same metal clustering problems as graphene. Therefore, it is possible that silicene could also be used for hydrogen storage like graphene, since there are similar properties between the two. Also, it is interesting to study how silicene would be different from graphene in terms of hydrogen interaction, since silicene, unlike graphene, has higher lattice constant along the planar lattice vectors and is not perfectly flat but has a buckled structure (Lin & Ni, 2012).

2. METHODOLOGY

Spin-polarized ground state density functional theory (DFT) calculations were done using the Vienna Ab-Initio Simulation Package (VASP), a plane wave-based code (Kresse & Furthmüller, 1996a, 1996b; Kresse & Hafner, 1993, 1994). The projector-augmented wave (PAW) method was used to describe the potentials (Blöchl, 1994; Kresse & Joubert, 1999). The Generalized Gradient Approximation (GGA) functional in the Perdew, Burke, and Ernzerhof (PBE) form was used to approximate the exchange-correlation energy (Perdew, Burke, & Ernzerhof, 1996, 1997). The k point mesh was automatically generated using the Monkhorst Pack scheme. Gaussian smearing with broadening width of 0.1 eV was used. For static calculations, the energy convergence criterion of 1x10⁻⁴ eV was used. The atoms were relaxed until the atomic forces were below 10⁻² eV/Å. For convergence test calculations involving one to two atoms, only the gamma point and default plane wave energy cutoff of metal was used. The static calculations to determine the silicene buckling height and lattice constant used an 11x11x11 gamma-centered k point mesh with a plane wave energy cutoff of 500 eV. Relaxation and static calculations used 7x7x1 k point mesh and 400 eV energy cutoff. The transition metals Co, Ni, Pd, and Pt were used for the metal decoration. The binding energy of the metal adatom with the silicene substrate was computed using the equation:

$$E_B = E_{S-M} - (E_S + E_M) \qquad \text{(Eq. 1)}$$

where:

E_B = Binding energy of metal adatom with silicene

E_{S-M} = Energy of metal-decorated silicene

E_S = Energy of pristine silicene
E_M = Energy of isolated metal adatom

Four adsorption sites were tested: the bridge site (B), hollow site (H), top site of the higher sublattice plane (T), and the valley site or the top site of the lower sublattice plane (V). Figure 1 shows the location of these four sites on a 4x4 silicene cell.
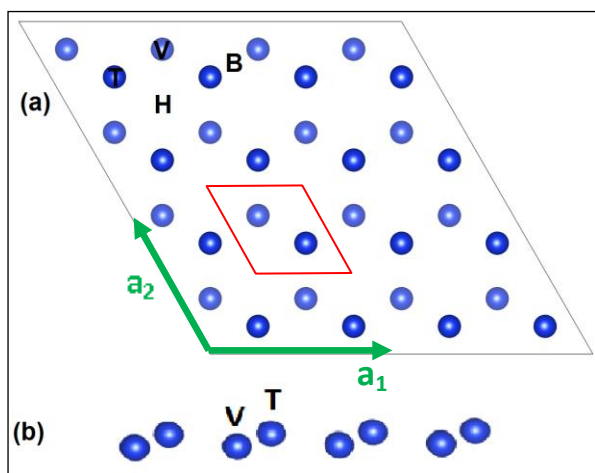

Fig. 1. (a) A 4x4 silicene cell showing the four possible adsorption sites. The primitive unit cell is enclosed in red box. This primitive cell is translated along the a_1 and a_2 lattice vectors to form the 4x4 silicene cell. (b) A side view of 4x4 silicene shows the distinction between the top site (T) and valley site (V).

For convergence tests involving isolated atoms, the cubic cell was used. For convergence test of silicene buckling height and lattice constant using static calculations, a 1x1 primitive rhombohedral cell was used (Fig. 1). The buckling height and lattice constant from these calculations were implemented in the relaxation calculations (which utilized a 4x4 unit cell) for finding the most stable metal adsorption site on silicene. A vacuum height of 18 Å was used for these calculations and dipole correction along the z-axis was implemented.

The results from VASP were visualized using the VESTA (Visualization for Electronic and Structural Analysis) software (Momma & Izumi, 2008, 2011). VESTA was also used to measure the distances between metal adsorbate and silicon atoms in the relaxed structure.

3. RESULTS AND DISCUSSION

3.1 Convergence Tests

Convergence tests were done to verify the optimal k point sampling mesh and plane wave energy cutoff of the system. For the k point sampling convergence test, the 4 x 4 pristine silicene was used since this system has larger dimensions than the isolated metal adatom. For the plane-wave energy cutoff convergence test, the metal adatoms were used since these elements required larger energy cutoff.

3.1.1 K point convergence test

The number of k points along the a_1 and a_2 lattice vectors (n_k) was increased from 1 to 12 with increment of one. The absolute value of the energy differences (ΔE) per increase in n_k was computed. Figure 2 shows the results. The consistent decrease in ΔE can be seen from the Fig. 2 (inset) starting from n_k=7. However, the energy difference that is comparable with 1meV was attained at n_k=8.
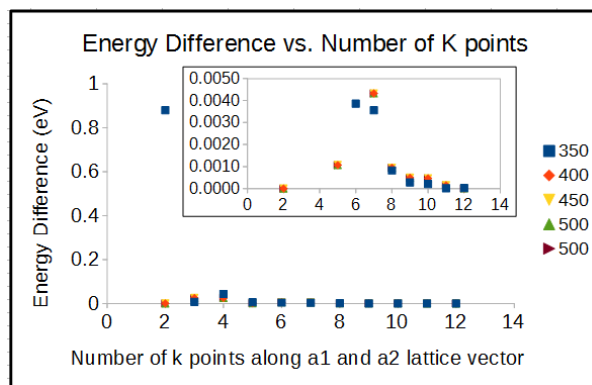

Fig. 2. The resulting energy differences vs. number of k points

3.1.2 Plane wave energy cutoff convergence test

The plane wave energy cutoff (E_{cut}) was varied from 150 to 500 eV with increment of 50 eV. The energy difference of ΔE was also computed. Figure 3 shows the results of this convergence test. A steady decrease in ΔE was observed as the E_{cut} was increased. The difference of 1meV was observed for E_{cut}=450eV, except for Pd, which required E_{cut}=500eV for an ΔE =1meV to be attained (Fig. 3, inset). The computed ΔE~2meV for Pd at E_{cut}=450eV can still be

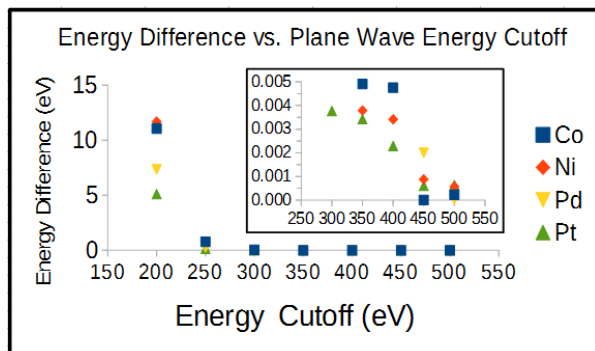considered to be an acceptable energy difference to attain accurate calculations.

Fig. 3. The resulting energy differences vs. plane wave energy cutoff.

Fig. 4. The ground state energy of silicene for different lattice parameter and buckling height combinations.

3.2 Determining the buckling height and lattice constant of silicene

The buckling height (Δz) and lattice constant (α) along the a_1 and a_2 directions were determined using static calculations. The lattice constant was varied from 3.78 Å to 4.00 Å, with increment of 0.01 Å, while Δz was varied from 0.40 Å to 0.54 Å, with increment of 0.01 Å The energy from different combinations of these parameters was calculated. The energy of a flat silicene ($\Delta z=0.00$ Å) with varying lattice constant was also calculated. The parameter combination that yielded the lowest energy is considered to be the most stable and the one that was used for the succeeding calculations. Figure 4 shows how the energy varies for different lattice constant and buckling height values. It can be easily seen that the flat silicene is the most unstable among the different systems (Fig. 4, inset). The figure shows that very close minima are obtained from different Δz –α combinations. A closer examination shows that the lowest energy was obtained for α=3.87 Å and Δz=0.45 Å. Hence, these values were used for the relaxation calculations (Sec. 3.3) in determining the optimal binding site for the metal adsorbate.
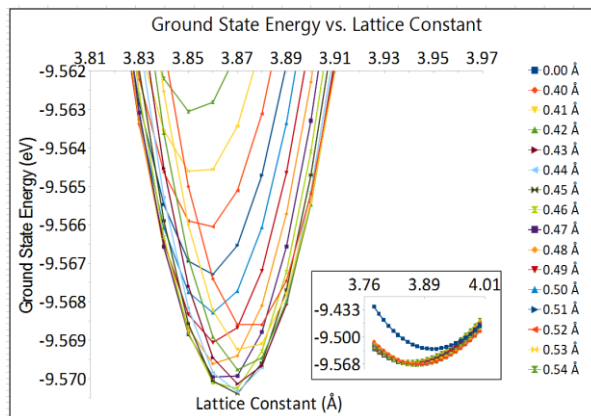
3.3 Verifying the most stable adatom site

Both relaxation and static calculations were used to verify the most stable metal adsorption site. For the relaxation calculations, the metal and silicon atoms were allowed to move but the cell size and shape were maintained constant. The adsorption site with the highest binding energy (E_b) is considered to be the most stable based from our definition in Eq. 1. For the static calculations, the silicon atoms are fixed and the height of metal adatom above the binding site (z) was varied. The calculated ground state energies for different heights and adsorption sites were compared. The minimum point is considered to be the most stable site for the metal adsorbate.

3.3.1 Relaxation Calculations

The computed E_b was used to calculate the ratio of the binding energy of metal adsorbate with silicene over the cohesive energy of the metal bulk (E_b/E_c). The standard value of E_c was used from Kittel (1996). A higher E_b/E_c ratio means that there will be lower possibility of adatom clustering, which would result in better H_2 uptake by the material. Table 1 shows the computed E_b/E_c ratio. The E_b/E_c results from the study of Lin & Ni (2012) was compared with our computed value. The distance of metal adatom with the nearest silicon atom (d_{M-Si}) was also obtained. Table 2 shows the computed d_{M-Si} values and the comparison with Lin and Ni's (2012) d_{M-Si} values.

Table 1. Binding Energy over Cohesive Energy Ratio for Metal-Decorated Silicene

Metal Adatom	Adsorption Site	E_b/E_c Calculated	E_b/E_c (Lin & Ni, 2012)	Diff
Co	B	0.865	-	-
	H	0.968	1.017	0.048
	T	0.835	0.896	0.061
	V	0.865	0.924	0.059
Ni	B	0.934	-	-
	H	1.070	1.076	0.006
	T	0.889	0.893	0.004
	V	0.934	0.939	0.005
Pd	B	0.965	-	-
	H	1.095	1.080	0.015
	T	0.910	0.898	0.012
	V	0.965	0.951	0.014
Pt	B	0.897	-	-
	H	1.004	1.005	0.001
	T	0.875	0.878	0.003
	V	0.897	0.899	0.002

Table 2. Smallest Metal-Silicon Bond Length (d_{M-Si})

Metal Adatom	Adsorption Site	d_{M-Si} Calculated	d_{M-Si} (Lin & Ni, 2012)	Diff
Co	B	2.27	-	-
	H	2.30	2.27	0.03
	T	2.26	2.29	0.03
	V	2.27	2.29	0.02
Ni	B	2.25	-	-
	H	2.32	2.31	0.01
	T	2.24	2.24	0.00
	V	2.25	2.25	0.00
Pd	B	2.42	-	-
	H	2.46	2.46	0.00
	T	2.41	2.42	0.01
	V	2.42	2.42	0.00
Pt	B	2.41	-	-
	H	2.43	2.42	0.01
	T	2.42	2.43	0.01
	V	2.41	2.41	0.00

3.3.1 Static Calculations

In addition with the relaxation calculations presented, static calculations were done to verify the optimal adsorption site for the metal adsorbate. Figures 5 to 8 show the results of these static calculations. If two sites have very close computed energy, the metal adatom may likely transfer to that adjacent site, until the minimum is reached. The

inset of Figs. 5 to 8 suggests a possible diffusion path of metal adatom towards the hollow site. In Fig. 5 (inset), the H site will most likely be preferred for the Co adatom from z>3.0Å. The atom may transfer to the V site at z=2.5Å, but it will again transfer to the hollow site at z=1.5 Å and will stay there since the energy of other adsorption sites will be very far from the H site.
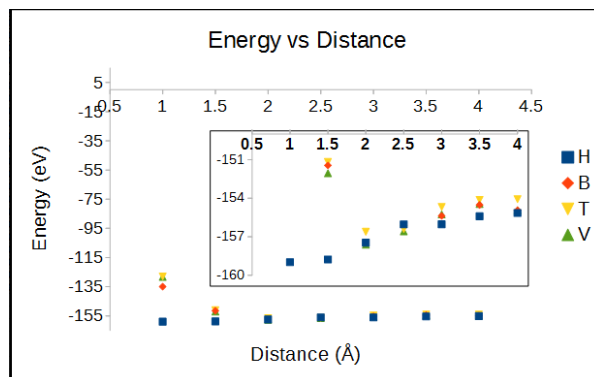

Fig. 5. Energy vs Distance above the adsorption site for Co.

The same can be seen for Ni (Fig. 6, inset). The Ni adatom may transfer sites at z>1.00Å, but will ultimately stay at H site since the energy of other sites are much higher than H at z=1.00 Å.
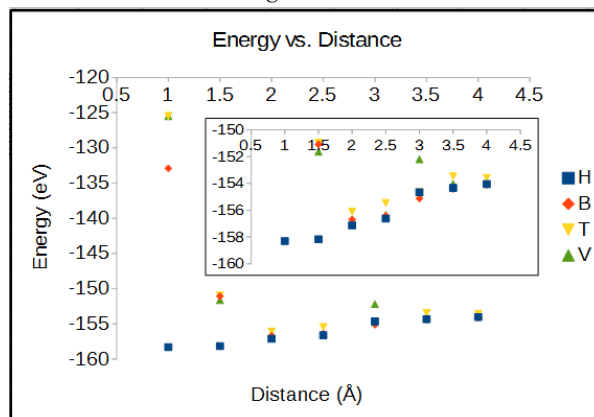

Fig. 6. Energy vs Distance above the adsorption site for Ni.

For the Pd and Pt adatoms (Fig.6-7, inset), it may move around the B, H, and V sites, at z>2.5 Å, but it will eventually transfer at the lowest point, which is the H site at z=1.5 Å.
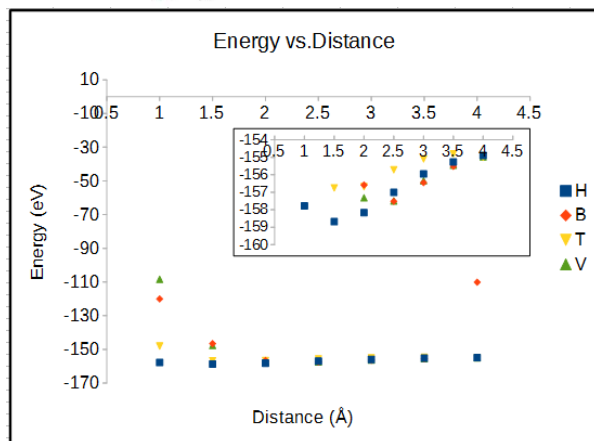
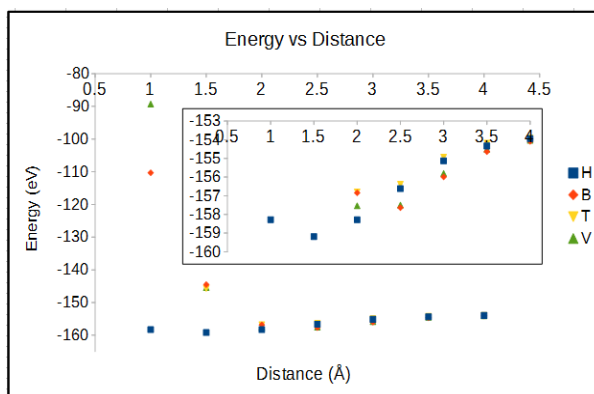Fig. 7. Energy vs Distance above the adsorption site for Pd.

Fig. 8. Energy vs Distance above the adsorption site for Pt.

The static calculations confirmed the results of relaxation calculations, which show the H site as the most stable adsorption site for the four metal atoms. It also suggests a possible diffusion path in silicene as the adatom moves towards the H site. However, there is a possibility that metal adatom may settle at a minimum other than the ones shown in Figs. 5 to 8, since the z increments used are relatively large (1.0Å) and the true minima for the adatoms may have been missed. Also, for the static calculations of Co and Ni, some computed energies did not meet the convergence criteria of 1×10^{-4} eV. Some of the Co and Ni calculations obtained energy differences (dE) of the orders 10^{-1} eV to 10^{-3} eV, which is higher than the typically accepted dE values, Hence, recalculation of these values are highly recommended.

3.4 H Interaction on Metal-Decorated Silicene

Calculations with the Pt-decorated silicene are currently ongoing. Initial ground state energy results encountered high dE values, which needs further recalculation. Afterwards, H interaction on silicene with other transition metal atoms will be done.

4. CONCLUSIONS

The adsorption site of Co, Ni, Pd, and Pt atoms on silicene was determined using DFT calculations. The relaxation calculations agreed with the previous study of Lin and Ni (2012) and showed the hollow site to be the most stable site for adsorption. Static calculations were also done and confirmed the relaxation results. The static calculations also suggested a possible diffusion path of metal adatom on silicene, but increasing the increment of z is recommended to ensure that the true energy minimum was not missed. Moreover, some of the static calculations for Co and Ni did not meet the energy convergence criterion and hence demand recalculation. Further studies on H_2 interaction with metal-decorated silicene are currently ongoing.

5. ACKNOWLEDGMENTS

6. REFERENCES

Blöchl, P. E. (1994). Projector augmented-wave method. Phys. Rev. B, 50(24), 17953–17979. doi:10.1103/PhysRevB.50.17953

Chen, C.-H., Chung, T.-Y., Shen, C.-C., Yu, M.-S., Tsao, C.-S., Shi, G.-N., … Lee, W.-L. (2013). Hydrogen storage performance in palladium-doped graphene/carbon composites. International

Journal of Hydrogen Energy, 38(9), 3681–3688. doi:10.1016/j.ijhydene.2013.01.070

Choi, M.-H., Min, Y.-J., Gwak, G.-H., Paek, S.-M., & Oh, J.-M. (2014). A nanostructured Ni/graphene hybrid for enhanced electrochemical hydrogen storage. Journal of Alloys and Compounds, 610, 231–235. doi:10.1016/j.jallcom.2014.04.206

Chu, S., Hu, L., Hu, X., Yang, M., & Deng, J. (2011). Titanium-embedded graphene as high-capacity hydrogen-storage media. International Journal of Hydrogen Energy, 36(19), 12324–12328. doi:10.1016/j.ijhydene.2011.07.015

Cipriani, G., Di Dio, V., Genduso, F., La Cascia, D., Liga, R., Miceli, R., & Ricco Galluzzo, G. (2014). Perspective on hydrogen energy carrier and its automotive applications. International Journal of Hydrogen Energy, 39(16), 8482–8494. doi:10.1016/j.ijhydene.2014.03.174

Converse, A. O. (2006). The impact of large-scale energy storage requirements on the choice between electricity and hydrogen as the major energy carrier in a non-fossil renewables-only scenario. Energy Policy, 34(18), 3374–3376. doi:10.1016/j.enpol.2005.08.001

Durbin, D. J., & Malardier-Jugroot, C. (2013). Review of hydrogen storage techniques for on board vehicle applications. International Journal of Hydrogen Energy, 38(34), 14595–14617. doi:10.1016/j.ijhydene.2013.07.058

Gao, Y., Zhao, N., Li, J., Liu, E., He, C., & Shi, C. (2012). Hydrogen spillover storage on Ca-decorated graphene. International Journal of Hydrogen Energy, 37(16), 11835–11841. doi:10.1016/j.ijhydene.2012.05.029

Gopalsamy, K., & Subramanian, V. (2014). Hydrogen storage capacity of alkali and alkaline earth metal ions doped carbon based materials: A DFT study. International Journal of Hydrogen Energy, 39(6), 2549–2559. doi:10.1016/j.ijhydene.2013.11.075

Guo, G. F., Huang, H., Xue, F. H., Liu, C. J., Yu, H. T., Quan, X., & Dong, X. L. (2013). Electrochemical hydrogen storage of the graphene sheets prepared by DC arc-discharge method. Surface and Coatings Technology, 228, S120–S125. doi:10.1016/j.surfcoat.2012.07.016

Höök, M., & Tang, X. (2013). Depletion of fossil fuels and anthropogenic climate change—A review. Energy Policy, 52, 797–809. doi:10.1016/j.enpol.2012.10.046

IEA. (2014). Key World Energy Statistics. IEA.

Kim, D., Lee, S., Hwang, Y., Yun, K.-H., & Chung, Y.-C. (2014). Hydrogen storage in Li dispersed graphene with Stone–Wales defects: A first-principles study. International Journal of Hydrogen Energy, 39(25), 13189–13194. doi:10.1016/j.ijhydene.2014.06.163

Kittel, C. (1996). Introduction to Solid State Physics (7th ed.).

Kresse, G., & Furthmüller, J. (1996a). Efficiency of ab-initio total energy calculations for metals and semiconductors using a plane-wave basis set. Computational Materials Science, 6(1), 15 – 50. doi:http://dx.doi.org/10.1016/0927-0256(96)00008-0

Kresse, G., & Furthmüller, J. (1996b). Efficient iterative schemes for ab initio total-energy calculations using a plane-wave basis set. Phys. Rev. B, 54(16), 11169–11186. doi:10.1103/PhysRevB.54.11169

Kresse, G., & Hafner, J. (1993). Ab initio molecular dynamics for liquid metals. Phys. Rev. B, 47(1), 558–561. doi:10.1103/PhysRevB.47.558

Kresse, G., & Hafner, J. (1994). Ab initio molecular-dynamics simulation of the liquid-metal\char21amorphous-semiconductor transition in germanium. Phys. Rev. B, 49(20), 14251–14269. doi:10.1103/PhysRevB.49.14251

Kresse, G., & Joubert, D. (1999). From ultrasoft pseudopotentials to the projector augmented-wave method. Phys. Rev. B, 59(3), 1758–1775. doi:10.1103/PhysRevB.59.1758

Lin, X., & Ni, J. (2012). Much stronger binding of metal adatoms to silicene than to graphene: A first-principles study. Physical Review B, 86(7). doi:10.1103/PhysRevB.86.075440

Li, Y., Zhao, G., Liu, C., Wang, Y., Sun, J., Gu, Y., … Zeng, Z. (2012). The structural and electronic properties of Li-doped fluorinated graphene and its application to hydrogen storage. International Journal of Hydrogen Energy, 37(7), 5754–5761. doi:10.1016/j.ijhydene.2011.12.146

Ma, L., Zhang, J.-M., Xu, K.-W., & Ji, V. (2014). Hydrogen adsorption and storage on palladium-Decorated graphene with boron dopants and vacancy defects: A first-principles study. Physica E: Low-Dimensional Systems and Nanostructures. doi:10.1016/j.physe.2014.09.022

Midilli, A., & Dincer, I. (2008). Hydrogen as a renewable and sustainable solution in reducing global fossil fuel consumption. International Journal of Hydrogen Energy, 33(16), 4209–4222. doi:10.1016/j.ijhydene.2008.05.024

Momirlan, M., & Veziroglu, T. (2005). The properties of hydrogen as fuel tomorrow in sustainable energy system for a cleaner planet. International Journal of Hydrogen Energy, 30(7), 795–802. doi:10.1016/j.ijhydene.2004.10.011

Momma, K., & Izumi, F. (2008). ıt VESTA: a three-dimensional visualization system for electronic and structural analysis. Journal of Applied Crystallography, 41(3), 653–658. doi:10.1107/S0021889808012016

Momma, K., & Izumi, F. (2011). ıt VESTA3 for three-dimensional visualization of crystal, volumetric and morphology data. Journal of Applied Crystallography, 44(6), 1272–1276. doi:10.1107/S0021889811038970

Nachimuthu, S., Lai, P. J., & Jiang, J.-C. (2014). Efficient hydrogen storage in boron doped graphene decorated by transition metals - A first-principles study. Carbon, 73, 132–140.

Najjar, Y. S. H. (2013). Hydrogen safety: The road toward green technology. International Journal of Hydrogen Energy, 38(25), 10716–10728. doi:10.1016/j.ijhydene.2013.05.126

Perdew, J. P., Burke, K., & Ernzerhof, M. (1996). Generalized Gradient Approximation Made Simple. Phys. Rev. Lett., 77(18), 3865–3868. doi:10.1103/PhysRevLett.77.3865

Perdew, J. P., Burke, K., & Ernzerhof, M. (1997). Generalized Gradient Approximation Made Simple [Phys. Rev. Lett. 77, 3865 (1996)]. Phys. Rev. Lett., 78(7), 1396–1396. doi:10.1103/PhysRevLett.78.1396

Pudukudy, M., Yaakob, Z., Mohammad, M., Narayanan, B., & Sopian, K. (2014). Renewable hydrogen economy in Asia – Opportunities and challenges: An overview. Renewable and Sustainable Energy Reviews, 30, 743–757. doi:10.1016/j.rser.2013.11.015

Sharaf, O. Z., & Orhan, M. F. (2014). An overview of fuel cell technology: Fundamentals and applications. Renewable and Sustainable Energy Reviews, 32, 810–853.

Sigal, A., Rojas, M. I., & Leiva, E. P. M. (2011). Interferents for hydrogen storage on a graphene sheet decorated with nickel: A DFT study. International Journal of Hydrogen Energy, 36(5), 3537–3546. doi:10.1016/j.ijhydene.2010.12.024

Ströbel, R., Garche, J., Moseley, P. T., Jörissen, L., & Wolf, G. (2006). Hydrogen storage by carbon materials. Journal of Power Sources, 159(2), 781–801. doi:10.1016/j.jpowsour.2006.03.047

Vogt, P., De Padova, P., Quaresima, C., Avila, J., Frantzeskakis, E., Asensio, M. C., … Le Lay, G. (2012). Silicene: Compelling Experimental Evidence for Graphenelike Two-Dimensional

Silicon. Physical Review Letters, 108(15). doi:10.1103/PhysRevLett.108.155501

Wang, H., Yuan, X., Wu, Y., Huang, H., Peng, X., Zeng, G., … Ren, M. (2013a). Graphene-based materials: Fabrication, characterization and application for the decontamination of wastewater and wastegas and hydrogen storage/generation. Advances in Colloid and Interface Science, 195-196, 19–40. doi:10.1016/j.cis.2013.03.009

Wang, H., Yuan, X., Wu, Y., Huang, H., Peng, X., Zeng, G., … Ren, M. (2013b). Graphene-based materials: Fabrication, characterization and application for the decontamination of wastewater and wastegas and hydrogen storage/generation. Advances in Colloid and Interface Science, 195-196, 19–40. doi:10.1016/j.cis.2013.03.009

Yadav, S., Zhu, Z., & Singh, C. V. (2014). Defect engineering of graphene for effective hydrogen storage. International Journal of Hydrogen Energy, 39(10), 4981–4995. doi:10.1016/j.ijhydene.2014.01.051

Yang, S. J., Jung, H., Kim, T., & Park, C. R. (2012). Recent advances in hydrogen storage technologies based on nanoporous carbon materials. Progress in Natural Science: Materials International, 22(6), 631–638. doi:10.1016/j.pnsc.2012.11.006

Zhou, H., Liu, X., Zhang, J., Yan, X., Liu, Y., & Yuan, A. (2014). Enhanced room-temperature hydrogen storage capacity in Pt-loaded graphene oxide/HKUST-1 composites. International Journal of Hydrogen Energy, 39(5), 2160–2167. doi:10.1016/j.ijhydene.2013.11.109

Züttel, A., Wenger, P., Sudan, P., Mauron, P., & Orimo, S. (2004). Hydrogen density in nanostructured carbon, metals and complex materials. Materials Science and Engineering: B, 108(1-2), 9–18. doi:10.1016/j.mseb.2003.10.087